JOC The Journal of Organic Chemistry

pubs.acs.org/joc Article

# One-Step Synthesis of 4-Octyl Itaconate through the Structure Control of Lipase

Changsheng Liu, Yilin Wang, Jiahao Liu, An'nan Chen, Juntao Xu, Renwei Zhang, Fang Wang, Kaili Nie,* and Li Deng*

Cite This: J. Org. Chem. 2021, 86, 7895−7903 Read Online

ACCESS | Metrics & More | Article Recommendations | Supporting Information

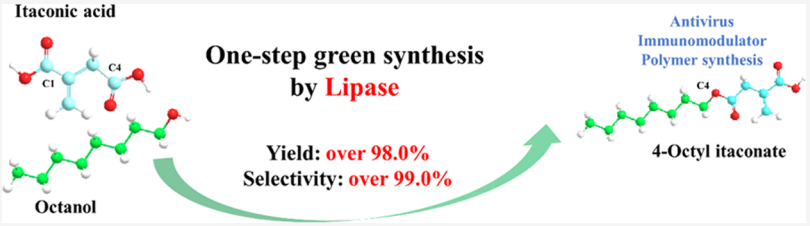


**ABSTRACT:** 4-Octyl itaconate is a novel antiviral and immunoregulatory small molecule showing great potential in the treatment of various autoimmune diseases and viral infections. It is difficult to selectively esterify the C4 carboxyl group of itaconate acid via one-step direct esterification using chemical catalysts, while the two-step route with itaconic anhydride as an intermediate is environmentally unfriendly and costly. This research investigated the one-step and green synthesis of 4-octyl itaconate through the structure control of lipase, obtaining 4-octyl itaconate with over 98% yield and over 99% selectivity. Multiscale molecular dynamics simulations were applied to investigate the reaction mechanism. The cavity pocket of lipases resulted in a 4-octyl itaconate selectivity by affecting distribution of substrates toward the catalytic site. Toluene could enhance monoesterification in the C4 carboxyl group and contribute to a nearly 100% conversion from itaconate acid into 4-octyl itaconate by adjusting the catalytic microenvironment around the lipase, producing a shrinkage effect on the channel.



## INTRODUCTION

Itaconic acid (IA) and its derivates are important compounds in polymers, agro-chemicals, and drug production.[1] Recently, research has demonstrated that itaconic acid has potent anti-inflammatory, antimicrobial,[2] and antiviral effects.[3] The immunity regulation of itaconic acid relies on its $\alpha,\beta$-unsaturated carboxylic acid to alkylate the key cysteine residues by Michael addition.[4] However, the natural form of itaconic acid is too hydrophilic to cross the lipid bilayer.[5]

4-Octyl itaconate (4-OI) is a cell-permeable itaconate derivative[4] with a free $\alpha,\beta$-unsaturated carboxylic acid near the terminal carbon, which mimics the endogenous itaconate better than other itaconate derivatives toward electrophilicity.[4,5] 4-OI has great potential in treating various autoimmune diseases,[6] such as multiple sclerosis (MS),[7] psoriasis,[8] and lupus erythematosus.[9] Even more enticing is that 4-OI shows a potent antiviral and anti-inflammatory activity toward SARS-CoV2 and various human pathogenic viruses.[10] 4-OI has anti-inflammation and antivirus efficacy[10] to treat virtual replication and the cytokine storm.[11] Besides, 4-OI is also valuable in renewable polymer synthesis,[12] such as poly(mono-*n*-octyl itaconate)[13] and maleic anhydride-mono-octyl itaconate copolymers.

However, the current synthesis route of 4-OI has low selectivity and low yield or is environmentally unfriendly and costly. The reported one-step synthesis under acidic conditions led to a low yield and poor selectivity (Scheme 1). The two-step synthesis route showed a high selectivity of 94% 4-OI with 95% yield,[14] while generation of the intermediate (itaconic anhydride), which was susceptible to hydrolysis during storage, in the two-step route was costly. The production process of itaconic anhydride, moreover, required an acid catalyst, a high-temperature condition, and an extensive subsequent purification step, thus increasing the pollution potential and production costs (Scheme 1). Being environmentally friendly, an efficient one-step synthesis route of 4-OI with high regioselectivity would accelerate its medical research in immunoregulation and application in polymer synthesis.

Development of biocatalysis may provide new insights into the one-step synthesis of 4-OI. Compared with chemical catalysts, lipases are well known for their high regioselectivity,[15] high catalytic activity,[16] and environmentally friendly reaction conditions.[17] Hence, lipases have been widely used in

Received: December 29, 2020
Published: June 4, 2021





https://doi.org/10.1021/acs.joc.0c02995
J. Org. Chem. 2021, 86, 7895−7903

Scheme 1. Synthesis Route of 4-OI

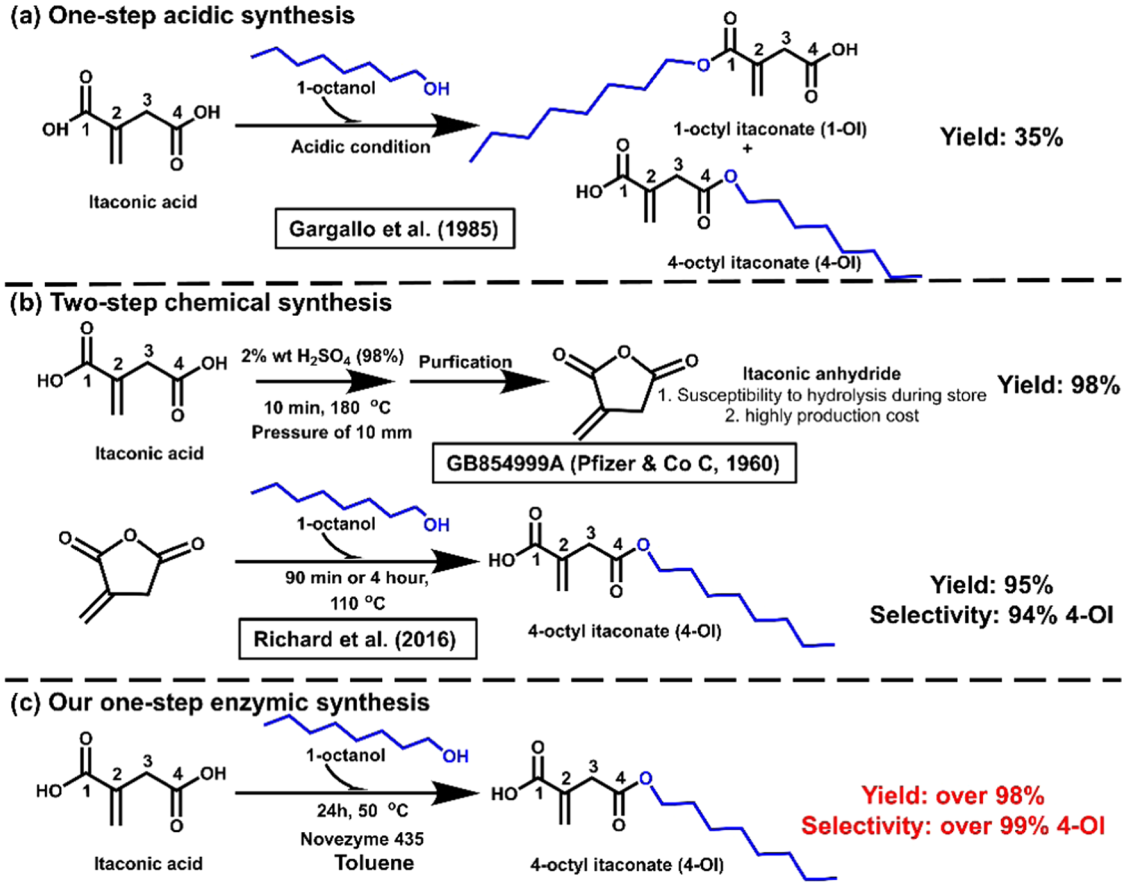


sustainable and green production.[18] The selectivity of lipases relies on the cavity shape and residue compositions in the pocket,[19] which may improve monoesterification in the C4 carboxyl group of IA. Sun et al. reported the selective amidation route of phenylglycinol by Novozym 435 (CALB), where the specific cavity shape contributed to high chemoselectivity for amidation (89.41%) rather than esterification (0.21%).[20] Hamberg et al. reported a site-directed mutagenesis strategy to improve the regioselectivity of CALB toward monoacylation from diols by changing the key residue compositions.[21] Meanwhile, solvents could influence the catalytic microenvironment and adjust the selectivity of enzymes, including substrate, stereo-, regio-, and chemoselectivity.[22] Duan et al. reported that the increase of the solvent log $P$ could improve the regioselectivity of CALB toward the *sn*-2 hydroxyl of a glycerol molecule, rather than the *sn*-1 position.[23] Bellot et al. also found that the increase in solvent polarity by adding a *n*-hexane/2-methyl-2-butanol equal-volume mixture improves the selectivity toward monoglyceride from 6 to 94% (molar percentage) in esterification between glycerol and oleic acid by *Rhyzomucor miehei* lipase.[24]

Based on the drawbacks of acid-catalyzed synthesis of 4-OI, a one-step green synthesis route of 4-OI based on the regioselectivity of enzymes was developed. Meanwhile, the catalytic microenvironment was improved to enhance this process. Molecular dynamics (MD) simulation was utilized to illustrate the mechanism of the high regioselectivity in this process. Compared with the traditional route using itaconic anhydride as the intermediate, this method reduced the operation steps and the production costs, improved the chemical sustainability, and provided a green, alternative way for the synthesis of 4-OI.

## RESULTS AND DISCUSSION

**Optimization of Reaction Conditions.** Esterification of IA is a cascade process, where IA is converted to mono-octyl itaconate (MOI) and the generated MOI is later esterified to di-octyl itaconate (DOI) (Figure S3). The composition of MOI and DOI in the final product was determined by reaction kinetics, expressed as the production rate of MOI ($V_{MOI}$) and the generation rate of DOI ($V_{DOI}$), as well as their ratio (Figure S3). As shown in Figure 1a, $H_2SO_4$ catalyzed the cascade esterification persistently without any selectivity toward MOI and Novozym 435 (CALB) to produce the highest MOI of 42%. The optimal CALB dosage was 50 wt % to IA, yielding 82% 4-OI at 24 h (Figure 1b). A higher dosage of lipases can provide more catalytic active sites, accelerating $V_{MOI}$ and $V_{DOI}$ synchronously (Figure S3). As a result, the yield of MOI increased and the monoester ratio (MER) decreased. On extending the reaction time, the accumulation of MOI in the reaction system accelerates $V_{DOI}$ and reduces $V_{MOI}$ (Figure S3), reducing the MER (Figure 1c). The time course curve showed that the highest yield of MOI (91%) appeared at 36 h. A similar observation was found in the lipase-catalyzed production of monoacylglycerol (MAG) from pinolenic acid and glycerol, where the increase of lipase dosage and reaction time increased the production of the byproduct, diacylglycerol (DAG).[25]

The substance molar ratio always shows a profound effect on the lipase-induced reaction.[26] Theoretically, more octanol


https://doi.org/10.1021/acs.joc.0c02995
J. Org. Chem. 2021, 86, 7895−7903

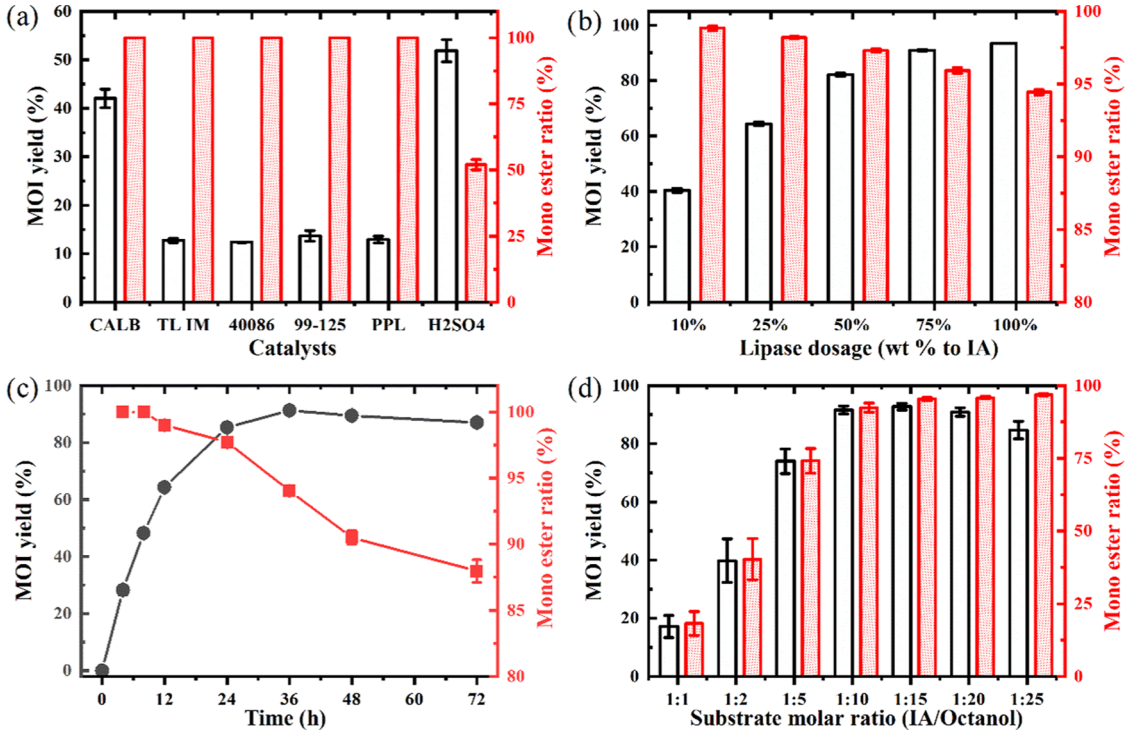


**Figure 1.** Optimization of various parameters in the enzymatic synthesis route. (a) Catalysts (0.01 g of lipases or 0.1 wt % sulfuric acid, concentration of itaconic acid is 0.64 mol·L$^{-1}$, concentration of 1-octanol is 6.4 mol·L$^{-1}$, 24 h), (b) lipase dosage (0.01−0.1 g of Novozym 435, concentration of itaconic acid is 0.64 mol·L$^{-1}$, concentration of 1-octanol is 6.4 mol·L$^{-1}$, 24 h), (c) time course (0.05 g of Novozym 435, concentration of IA is 0.64 mol·L$^{-1}$, concentration of 1-octanol is 6.4 mol·L$^{-1}$, 6−72 h), and (d) substrate molar ratio (0.05 g of Novozym 435, concentration of IA is 0.256−6.4 mol·L$^{-1}$, concentration of 1-octanol is 6.4 mol·L$^{-1}$, 36 h). All reactions were performed with 0.769 mmol of IA as the substrate at 50 °C and at 800 rpm.

facilitates the production of DOI and reduces the MER (Figure S3). Pereira et al. reported that an increase of lauric acid enhanced the production of di- and trilaurin in the cascade esterification of glycerol and lauric acid.[27] Intriguingly, lipase-mediated cascade esterification in this work showed an inverse phenomenon, where more octanol resulted in less DOI and yielded a higher MER (Figure 1d). We assume that excessive octanol may act as a solvent to influence cascade esterification.

**Computational Studies of the Selectivity toward MOI in CALB.** Unlike the acid catalyst, CALB selectively synthetized MOI (Figure 1a). In lipase-catalyzed esterification, the first step was the attack of the carboxyl group toward the hydroxyl oxygen of Ser105, forming the first tetrahedral intermediate (Figure S4).[28] Interestingly, the generated MOI would become a competitive substrate for IA, further affecting the composition of the final product. We investigated the movement of IA and MOI in the cavity pocket, and the enzymatic conformation was stable after 5000 ps (Figure S5), shown as a convergent root mean square deviation (RMSD) value.[29] Figure 2a shows that IA was more likely to form an acyl complex with the hydroxyl oxygen of Ser105 (0.4 nm) than MOI (1.0 nm). Furthermore, the independent gradient model (IGM)[30] showed that IA (Figure 2b) had stronger nonbonded interactions (blue, H bonds) with Thr40, Ser105, Gln106, Gln157, and Ile189, while MOI only had weak nonbonded interactions (green vdW) with surrounding residues (Figure 2c). Besides, the larger spatial size of MOI blocks its approach toward Ser105. Finnveden et al. reported similar observations in the esterase-catalyzed monosubstitution of divinyl adipate (DVA),[31] where the restricted space of esterase blocked the generated monosubstituted products from continuing to the next disubstituted reaction. Thus, IA was a better competitor than MOI to bind the catalytic site and proceed with the esterification process, matching the phenomenon of MOI high accumulation in the experiment.

**Computational Assay of the Effect of Octanol on Cascade Esterification.** The distribution of IA/MOI around CALB lipase under more and fewer octanol molecules was researched. The trajectory of RMSD in this conformation remained steady after 5000 ps, indicating the convergence of MD simulation results (Figure S6). With more octanol molecules (1000 octanol molecules), the $g(r)$ distribution of majority IA was concentrated in 2 nm (Figure 3a), while that of MOI appeared in 2.5 nm; as a result, IA was more likely to enter the cavity pocket than MOI to react. However, with fewer octanol molecules (100), IA and MOI were almost distributed in the same place, where they had a similar possibility to approach the cavity pocket (Figure 3b). The distribution of competitive substrates around the lipase further affects their reaction rate differently, agreeing with results in Figure 1d. The enhanced diffusion of substances from the lipase surface was also reported by Cao et al.,[29] where glucose could improve diffusion of harmful methanol molecules away from lipases and yield a protective effect. In this work, excess octanol ($\log P$ = 2.64) created a hydrophobic environment to influence the microscopic distribution of IA ($\log P$ = −0.26) and MOI ($\log P$ = 2.91) around lipases. Octanol not only affects the reaction kinetics as the substrate but also acts as a solvent to adjust the catalytic microenvironment of lipases.

**Influence of Solvents.** Inspired by octanol's role as a solvent, a variety of solvents with $\log P$ ranging from −1.3 to 4 were investigated in esterification of MOI. Application of



https://doi.org/10.1021/acs.joc.0c02995
J. Org. Chem. 2021, 86, 7895−7903

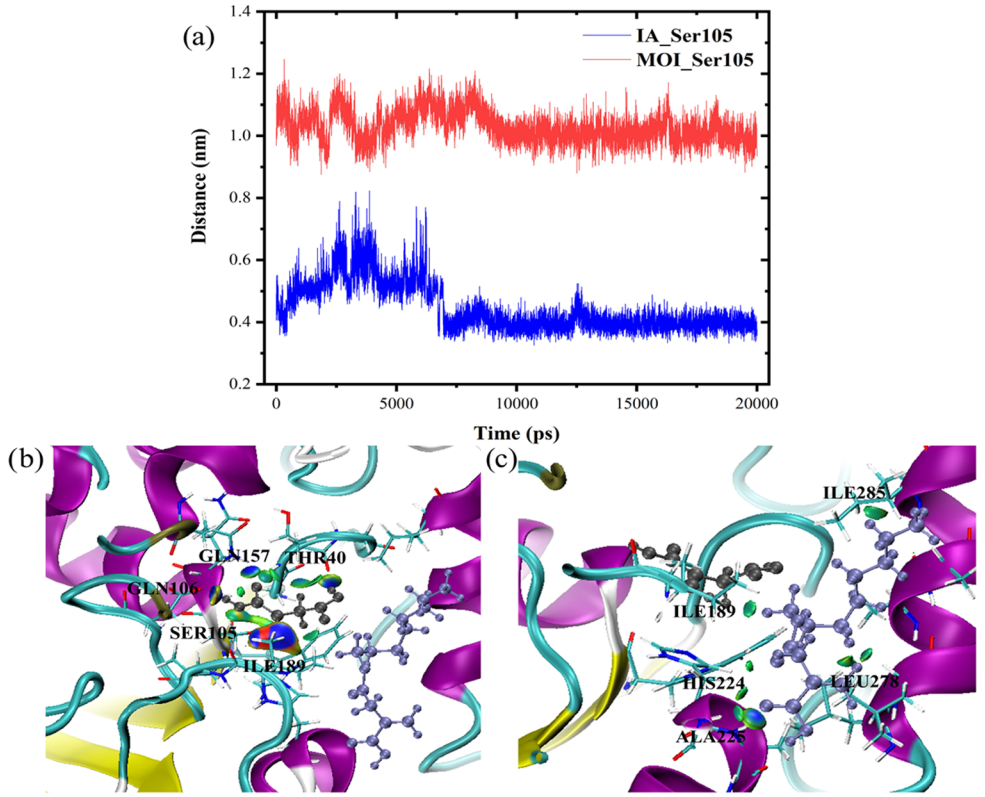


**Figure 2.** Distribution of IA/MOI in the cavity pocket. (a) MD results of the distance between IA/MOI and hydroxyl oxygen of Ser105 (IA, blue; MOI, red), (b) IGM analysis of IA, and (c) IGM analysis of MOI. (IGM, blue, represents strong nonbonded interactions, such as H bonds and halogen bonds; green represents middle strong nonbonded interactions, such as van der Waals (vdW) interactions; and red represents steric effects, such as ring tension and steric hindrance.)

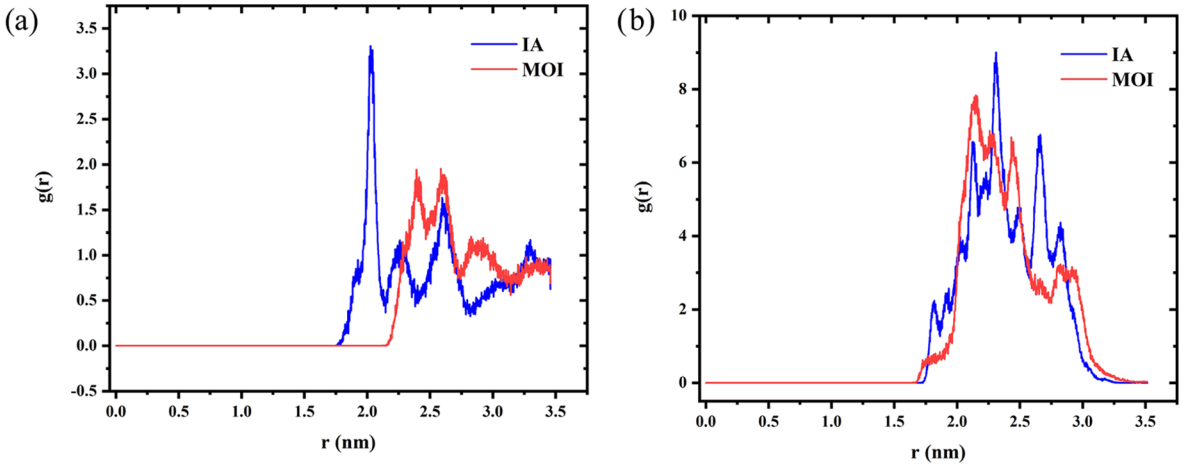


**Figure 3.** $g(r)$ Distribution of IA/MOI around the enzyme. MD results of the distance between IA/MOI and the centroid of lipase with (a) 1000 octanol molecules (IA, blue; MOI, red) and (b) 100 octanol molecules (IA, blue; MOI, red).

organic solvents in the lipase-catalyzed reaction has been widely researched, which could improve the solubility of hydrophobic substrates, help the recovery and reusability of lipases, favor the synthesis over hydrolysis, improve the mass transfer, and alter the regioselectivity of lipases.[32,33] However, solvents also affect the enzymatic activity by altering the critical water layer and the protein structure, especially the cavity pocket and active sites.[33] Figure 4 shows that toluene (TOL, log $P$ = 2.68) contributed to the highest yield of 99% MOI and the optimal toluene/octanol ratio was 1:1 (v/v) (Figure S7). To make the process more economical, recyclability under the optimal condition was investigated, where lipase can be reused for 16 batches with over 90% yield of MOI (Figure S8). TOL exerted a profound effect on production of MOI by increasing the yield and the MER.

**Mechanism of the CALB Regioselectivity on 4-OI in Silico.** This route showed a good performance in a 5 g scale-up reaction with over 98% yield, and MOI with 94% purity can be obtained (Table S1) through a series of separation. $^{1}$H NMR (Figure S10), $^{13}$C NMR (Figure S11), and heteronuclear multiple bond correlation (HMBC; Figures S2 and S12) revealed that our product was 4-OI with over 99% selectivity


https://doi.org/10.1021/acs.joc.0c02995
J. Org. Chem. 2021, 86, 7895−7903

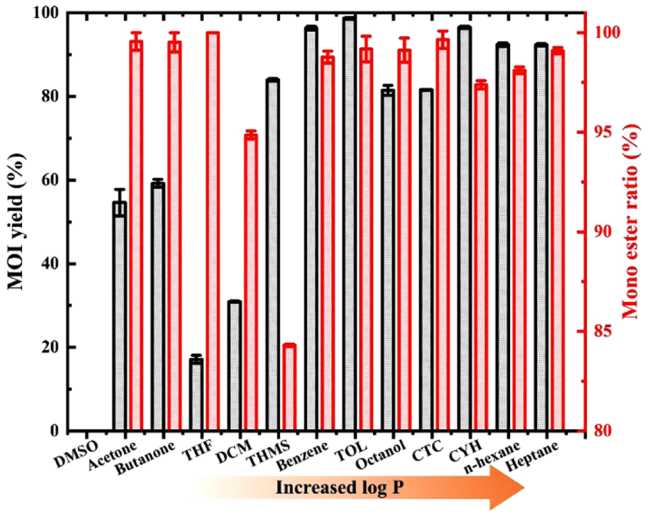


**Figure 4.** Effect of organic solvent on the yield of MOI and MER (solvent/octanol = 1:1 v/v). All reactions were performed using 0.05 g of Novozym 435, concentration of IA is 0.32 mol·L$^{-1}$, and concentration of 1-octanol is 3.2 mol·L$^{-1}$ (octanol group, concentration of 1-octanol is 6.4 mol·L$^{-1}$) at 50 °C, 800 rpm, and 24 h.

(Figure S1). In this reaction, both C4 and C1 are esterified, while esterification of C4 is dominant. The formation of the IA_Ser105 acyl complex and the attack of octanol are necessary phases in the esterification process (Figure S4).[28] Molecular docking results (Figure 5a) showed that the formation of the C4_Ser 105 complex could cling to the right side, where the C═C rigid bond was placed in a formed cleft (red arrow), and leave a channel for the attack of octanol. In the C4_Ser 105 complex, the distance between octanol and Ser105 was 3.4 Å, meeting the necessary distance requirement of 4 Å for a nucleophilic attack.[34] The hydrogen bond with Thr40 and hydrophobic interactions with surrounding residues, especially Ile189, Val190, Thr138, and Gln157, help to stabilize this conformation (Figure 5b). However, the formation of the C1_Ser 105 complex blocks the attack of octanol (Figure 5c) in the cavity pocket, yielding a 7 Å distance between the hydroxyl oxygen of octanol and Ser105 (interactions with surrounding residues are shown in Figure 5d). Ferrari et al. had similar findings where the catalytic cavity shape of CALB affected its selectivity in the peptide acylation reactions, especially its tightness and depth.[35]

Furthermore, GFN-FF MD was used to analyze the C4/C1 distribution in the active site. In this stable conformation after 40 ps (Figure S9), the C4 carboxyl group of IA was "closer" than the C1 carboxyl group to the hydroxyl oxygen of Ser105 (Figure 5f), indicating that C4 was more likely to interact with the Ser105 residue. Figure 5e shows that C4 had stronger nonbonded interactions (blue, H bonds) with Gly39, Gln106, and Ser105, while C1 only had middle nonbonded interactions with Val154 and Leu140 (green, vdW). Besides, the C═C bond could produce some vdW interactions with Thr40 and Ile238 to stabilize this conformation. Li et al. used a similar IGM to analyze the enzyme−peptide interaction, where H bonds and hydrophobic and vdW interactions contribute to the stable enzyme−peptide conformation.[36] Then, the C4 carboxyl group of IA is more likely to form an acyl complex

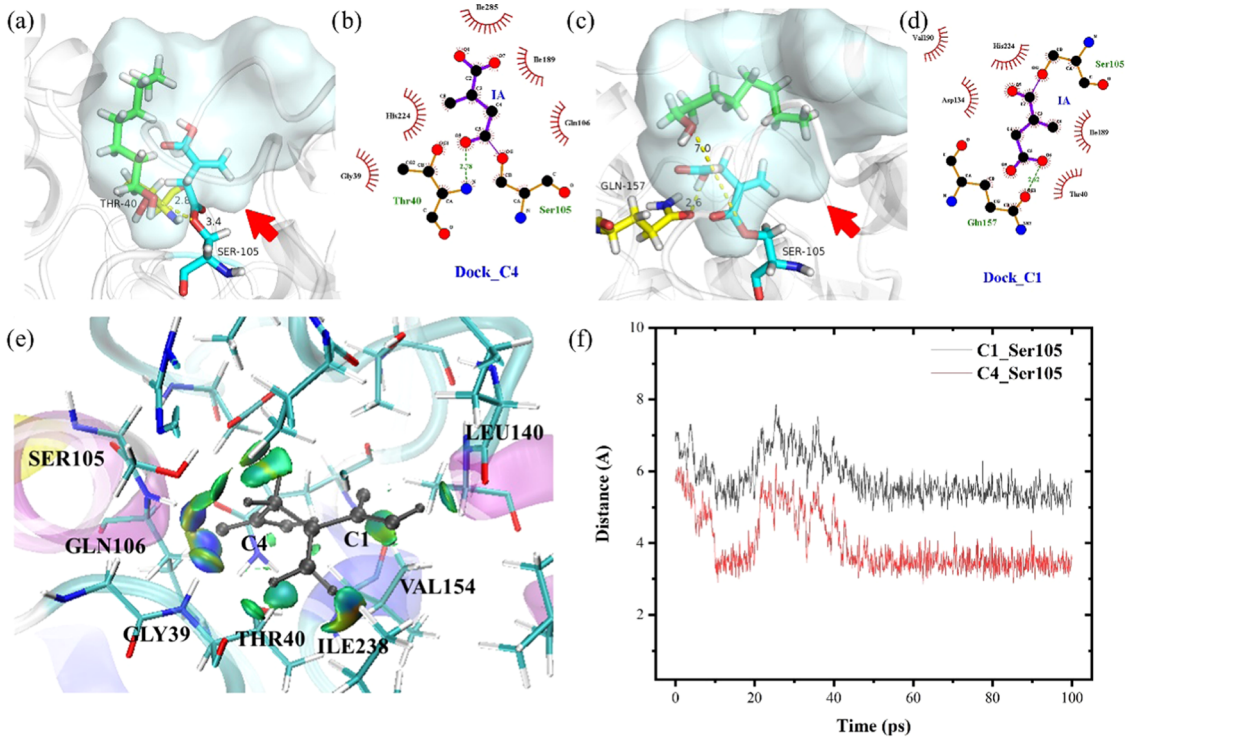


**Figure 5.** Regioselectivity from the cavity pocket toward 4-OI. (a) Docking result of the C4_Ser 105 complex; (b) C4_Ser 105 complex binding site, prepared with LigPlot +; (c) docking result of the C1_Ser 105 complex; (d) C1_Ser 105 complex binding site, prepared with LigPlot; (e) independent gradient model (IGM) analysis (blue represents strong nonbonded interactions, such as H bonds and halogen bonds; green represents middle strong nonbonded interactions, such as vdW interactions; red represents steric effects, such as ring tension and steric hindrance); and (f) MD results of the distance between C1/C4 and hydroxyl oxygen of Ser105.


https://doi.org/10.1021/acs.joc.0c02995
J. Org. Chem. 2021, 86, 7895−7903

with the Ser105 residue than the C1 carboxyl group and proceed with further esterification.

**Reaction Dynamics.** In this enzymatic synthesis process, the solvent environment performed an important role. TOL showed the best performance among solvents, improving the yield of MOI from about 85 to 99% with IA/octanol = 1:10 (molar ratio) at 24 h (Figure 4). Interestingly, TOL does not improve the production rate of all esterified products ($V_{MOI}$ and $V_{DOI}$) simultaneously. The addition of TOL could improve $V_{MOI}$ by 44.84% and decrease $V_{DOI}$ to 56.87%, further increasing the ratio between $V_{MOI}$ and $V_{DOI}$ from 88.43 to 225.20 (Table S2). Meanwhile, TOL could improve the $V_{max}$ of the MOI production rate by 637.35% and reduce the $V_{max}$ of the DOI production rate to 26.82% (Table S3). This opposite effect of TOL on $V_{MOI}$ and $V_{DOI}$ might be due to the enhanced diffusion of hydrophobic MOI from the cavity pocket to the external hydrophobic environment by TOL, matching the previous MD result in Figure 3a.

To further verify this hypothesis, we investigated the effect of mixed solvents with various log *P* values (Table S4) on 4-OI production (Figure 6). In a high log *P* environment (>2), MOI yield had a similar performance with over 90% yield, while the MER was reduced. TOL shows a better performance than the mixed solvent with similar log *P* values, although they have the same effect on adjusting microdistribution of substances. TOL may change the enzymatic conformation, especially the key residues, to improve both the catalytic activity and selectivity.

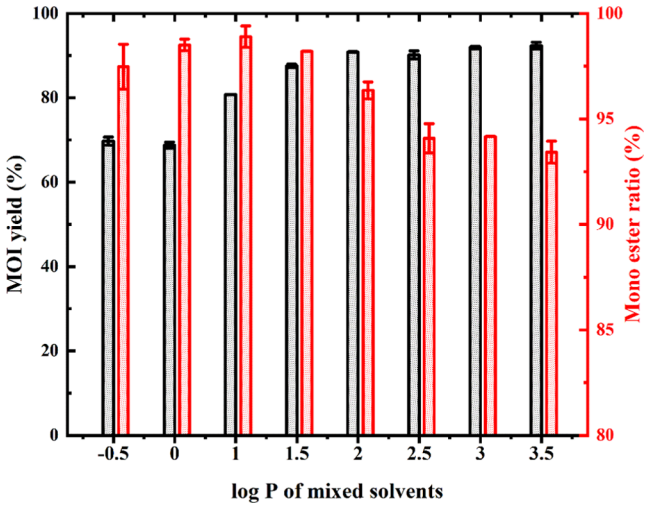


**Figure 6.** Effect of mixed solvent on the yield of MOI and MER (mixed solvent/octanol = 1:1 v/v). All reactions were performed using 0.05 g of Novozym 435, concentration of IA is 0.32 mol·L$^{-1}$, and concentration of 1-octanol is 3.2 mol·L$^{-1}$ at 50 °C, 800 rpm, and 24 h.

**Computational Analysis of TOL on the Cavity Pocket.** The computational results showed that TOL performed a structure control effect of the lipase. The cavity pocket of CALB was separated into two channels (Figure 7a) by two "saddle" residues of ILE189 and ILE285. However, the two channels were reduced to one in the TOL environment (Figure 7b). TOL has a shrinkage effect on the left channel by closing the distance between LEU144 and VAL286 residues (Figure 7d), while it does not affect the original saddle residues (Figure 7c) and the right channel. Thus, TOL could improve the selectivity of CALB toward 4-OI by shrinking the cavity (Figure 7d). The improvement effect of TOL on the MOI selectivity was investigated on other diacids (Figure 8). Interestingly, the side chain seems to be the key for the specific cavity pocket of CALB and TOL to improve MER. In the cascade esterification of succinic acid and 1-octanol, CALB did not exhibit selectivity toward the monoester, and the MER was lowered to less than 10% at 8 h. Besides, the addition of TOL did not improve the MER and it even lowered MER to almost 0 at 8 h (Figure 8b). However, for other diacids with side chains (malic acid, 2-methylglutaric acid, 2-methylsuccinci acid), CALB exhibited a higher MER at 8 h (87% malic acid monoester, 62% 2-methylglutaric acid monoester, 90% 2-methylsuccinci acid monoester). The addition of TOL further improves the monoester process, yielding 96% malic acid monoester at 8 h, 70% 2-methylglutaric acid monoester at 8 h, and 92% 2-methylsuccinci acid monoester at 8 h (Figure 8a,c,d).

## CONCLUSIONS

The present research demonstrated a one-step and green synthesis route of 4-octyl itaconate by the structure control of the lipase, yielding outstanding performances in yield and selectivity. The special cavity of CALB and the shrinkage effect of the solvent exhibited a nearly 100% direct conversion of 4-OI from IA and octanol, meeting the principles of green engineering in reducing operating steps and saving energy consumption. Under the optimal condition, 4-OI with over 98% yield and over 99% selectivity was obtained. Lipases can be reused for 16 batches with over 90% yield of 4-OI. A multiscale molecular simulation analysis was used to reveal the catalytic mechanism. First, the cavity pocket of CALB resulted in a 4-OI selectivity by affecting the acyl−enzyme complex conformation and microdistribution of C1/C4 and IA/MOI. Second, TOL could improve the 4-OI selectivity by affecting the substrate distribution of IA/MOI around the enzyme surface and performing a shrinkage effect. This strategy also applies to monoesterification of other diacids with side chains.

## EXPERIMENTAL SECTION

**Materials.** IA (99%) was obtained from TCI. 1-Octanol (99%) was obtained from Sigma-Aldrich. 4-Octyl itaconate (98%) standard was purchased from Ark. Dimethylsulfoxide (DMSO), acetone, butanone, tetrahydrofuran (THF), dichloromethane (DCM), trihalomethanes (THMS), benzene, toluene (TOL), octanol, carbon tetrachloride (CTC), cyclohexane (CYH), *n*-hexane, and heptane were of reagent grade. Novozym 435 (*Candida antarctica* lipase B immobilized on macroporous acrylic resin, CALB), Lipozyme TL IM (lipase from *Thermomyces lanuginosus*, immobilized on silica), and Novozym 40086 (lipase from *Rhizomucor miehei*, immobilized on acrylic resin) were purchased from Novozymes, Beijing, China. Porcine pancreas lipase (PPL) powder was purchased from Sigma Life Science, and *Candida sp.* 99-125 lipase powder was purchased from Beijing CAT New Century Biotechnology Co., Ltd.

**Esterification of Itaconic Acid.** IA (0.769 mmol) and 1-octanol (0.769−19.225 mmol) were added into a 4 mL brown glass bottle. In experimental groups containing organic solvents, various solvents (1.2 mL) were added to this bottle. The mixture was then preheated at 50 °C for 10 min. Catalysts (0.01−0.1 g of lipases or 0.5 wt % sulfuric acid) were added and the reaction was conducted in a thermostatic bath at 50 °C, 800 rpm, and 24−72 h. Samples (20 μL) were removed for gas chromatography (GC) analysis at various times after adding 1 mL of *n*-hexane and centrifuging at 8000 rpm for 3 min. All reactions were conducted at least in triplicate.

**Scale-Up Experiment and Separation of Mono-octyl Itaconate (MOI).** The scale-up experiment was conducted in a 250


https://doi.org/10.1021/acs.joc.0c02995
J. Org. Chem. 2021, 86, 7895−7903

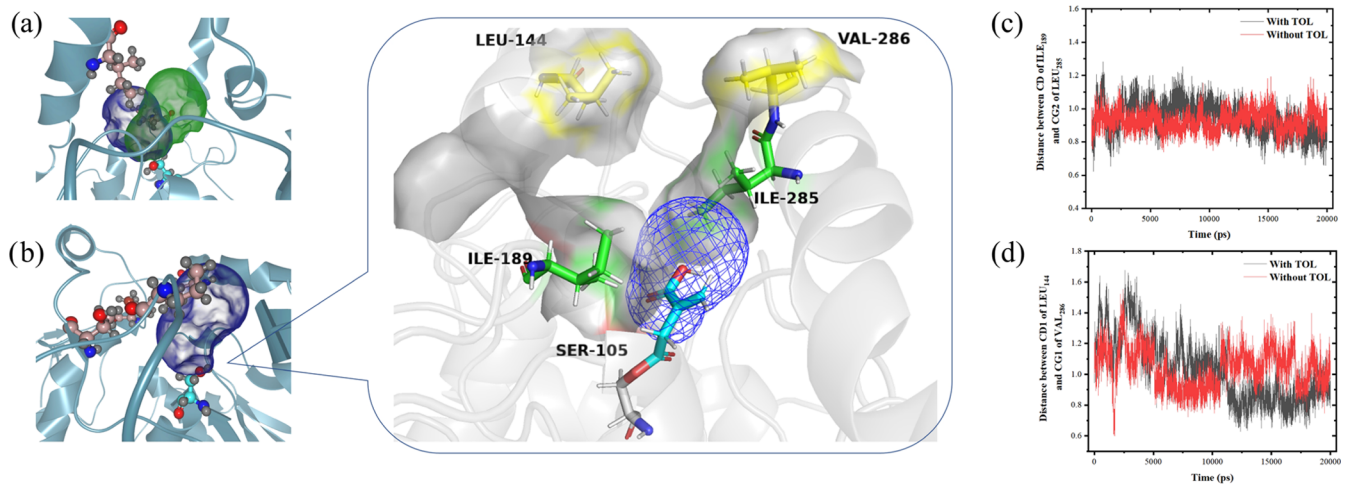


**Figure 7.** Assay of the solvent effect on the cavity pocket. (a) Cavity pocket without TOL, (b) cavity pocket with TOL, (c) distance between ILE189 and ILE285, and (d) distance between LEU144 and VAL286.

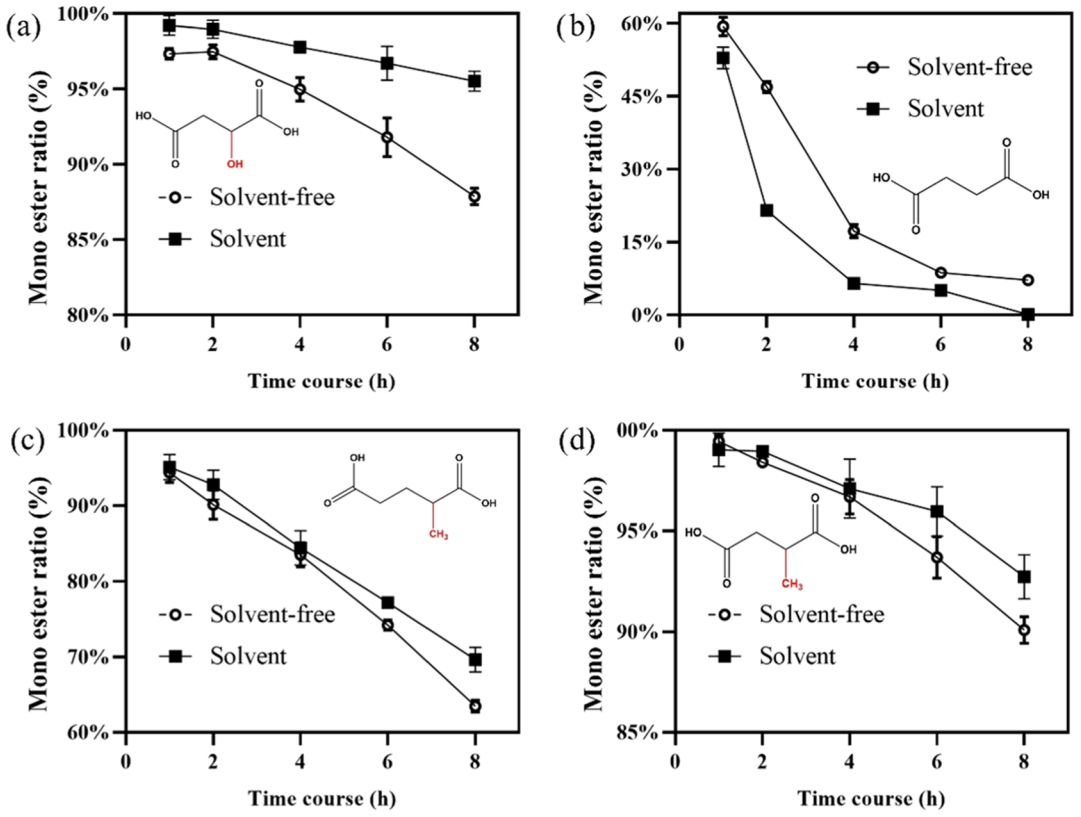


**Figure 8.** Application on other diacids. (a) malic acid, (b) succinic acid, (c) 2-methylglutaric acid, and (d) 2-methylsuccinci acid. All reactions were performed using 0.05 g of Novozym 435 at 50 °C, 800 rpm, and 24 h. The concentration of diacids and 1-octanol is 0.64 and 6.4 mol·L$^{-1}$, respectively, in the solvent-free system; the concentration of diacids and 1-octanol is 0.32 and 3.2 mol·L$^{-1}$, respectively, in the solvent system.

mL three-necked, round-bottom flask, with 2.5 g of Novozym 435, 5 g of IA (38.5 mmol), 50 g of 1-octanol (385 mmol), and 60 mL of TOL at 50 °C, 250 rpm, and 24 h. The reaction mixture was filtered to separate lipases. A 1:1 saturated NaCl salt solution (V/V) was added to remove the residual unreacted IA. The supernatant was collected and organic solvents were removed under vacuum. The residue containing only mono-octyl itaconate (MOI) and 1-octanol was separated by short-path distillation[37] under the following conditions: $T_{\text{Evaporation wall}}$ (°C) = 30, $T_{\text{cooling wall}}$ (°C) = 2, scraper speed (rpm) = 250, and pressure (Pa) = 0.1. 1-Octanol was removed as the light phase and a white solid product was obtained.

**GC Analysis.** A GC-2010 Plus (Shimadzu) gas chromatograph with an FID detector and a DB-1 chromatographic column (30 m × 0.25 mm, 0.1 $\mu$m, Agilent) was used to analyze samples. The temperatures of the injection port and the FID detector were set as 360 and 380 °C, respectively. The temperature programming of the column was set at 100 °C for 0.2 min; it was first increased to 165 °C at 8 °C·min$^{-1}$ and maintained for 1 min and then increased to 340 °C at 20 °C·min$^{-1}$ and maintained for 1.92 min.[17] Data including the yield of MOI and MER are calculated as wt %. MOI yield refers to the percentage of MOI among all reaction substances (IA, MOI, and DOI), while MER yield refers to the percentage of MOI between IA


https://doi.org/10.1021/acs.joc.0c02995
J. Org. Chem. 2021, 86, 7895−7903

esters (MOI and DOI). All of the data were the averages of triplicate experiments.

**NMR Identification.** The structure of the purified product was analyzed using $^{1}$H NMR and $^{13}$C NMR spectra and HMBC with a $CDCl_3$ solvent. All nuclear magnetic resonance (NMR) spectra were recorded on an Avance 600 spectrometer (600.13 MHz) equipped with a BBI probe head with a *z*-gradient from Brucker Biospin GmbH. All NMR data were processed and analyzed with MestReNova. Full $^{1}$H and $^{13}$C assignments were obtained at 25 °C from standard 1D experiments, as well as a two-dimensional (2D) correction experiment ($^{1}$H, $^{13}$C HMBC). The $^{1}$H and $^{13}$C chemical shifts were referenced against TMS. Chemical shifts for $^{1}$H and $^{13}$C NMR spectra are reported in ppm ($\delta$) relative to the residue protium in the solvent ($CDCl_3$: $\delta$ 7.26, 77.0 ppm, and the multiplicities are presented as follows: s = singlet, d = doublet, t = triplet, q quartet, m = multiplet, brs = broad single).

$^{1}$H NMR ($CDCl_3$, 600 MHz) $\delta$ 6.46 (s, 1H), 5.83 (s, 1H), 4.10 (t, 2H, $J$ = 6.7 Hz), 3.34 (s, 2H), 1.64−1.60 (m, 2H), 1.35−1.23 (m, 10H), 0.88 (t, 3 H, $J$ = 6.9 Hz).

$^{13}$C{1H} NMR ($CDCl_3$,150 MHz) $\delta$ 171.3, 170.6, 133.4, 130.6, 65.3, 37.3, 31.8, 29.2, 29.1, 28.5, 25.8, 22.6, 14.1.

$^{1}$H NMR and $^{13}$C NMR data were identical to the data in the literature.[5]

Based on NMR spectroscopy, our product was 4-OI, rather than 1-OI, which was consistent with previous reports.[4,14] 4-OI had chemical shifts in 6.46 and 5.83 ppm at $^{1}$H NMR, while 1-OI had chemical shifts in 6.36 and 5.74 ppm[14] at $^{1}$H NMR (Figure S1). Our products showed over 99% selectivity of 4-OI, and the 1% chemical shifts might be caused by DOI (Figure S1). To further identify the structure of our product, HMBC (1H detected heteronuclear multiple bond correlation) was conducted. The H5-C4 and H3-C4 interactions further revealed that our product was 4-OI (Figure S2).

**Assay of 4-OI Selectivity.** The cavity pocket of CLAB lipase (pdb: 5GV5) and the microenvironment jointly contributed to the high 4-OI selectivity. A multiscale molecular simulation analysis from perspectives of the acyl−enzyme complex structure, molecular dynamics (MD), IA/MOI distribution, and channel change was conducted to investigate their influence (shown in the SI).

## ■ ASSOCIATED CONTENT

### Supporting Information

The Supporting Information is available free of charge at https://pubs.acs.org/doi/10.1021/acs.joc.0c02995.

Detailed experimental methods, NMR data, separation data, and MD data; generation rate measurement; preparation of mixed solvents; multiscale molecular simulation analysis; IA/MOI distribution on the cavity pocket; catalytic mechanism of lipase (N435); effect of TOL dosage on the yield of MOI and selectivity; composition of the reaction liquid in each step; and the production rate of MOI/DOI in the solvent-free/solvent system (PDF)

## ■ AUTHOR INFORMATION


### Corresponding Authors

**Kaili Nie** − *Beijing Bioprocess Key Laboratory and State Key Laboratory of Chemical Resource Engineering, College of Life Science and Technology, Beijing University of Chemical Technology (BUCT), Beijing 100029, P. R. China;* orcid.org/0000-0002-0613-9850; Phone: +86-010-64414543; Email: niekl@mail.buct.edu.cn; Fax: +86-010-64416428

**Li Deng** − *Beijing Bioprocess Key Laboratory and State Key Laboratory of Chemical Resource Engineering, College of Life Science and Technology, Beijing University of Chemical Technology (BUCT), Beijing 100029, P. R. China;* orcid.org/0000-0001-8792-529X; Email: dengli@mail.buct.edu.cn

### Authors

**Changsheng Liu** − *Beijing Bioprocess Key Laboratory and State Key Laboratory of Chemical Resource Engineering, College of Life Science and Technology, Beijing University of Chemical Technology (BUCT), Beijing 100029, P. R. China*

**Yilin Wang** − *Beijing Bioprocess Key Laboratory and State Key Laboratory of Chemical Resource Engineering, College of Life Science and Technology, Beijing University of Chemical Technology (BUCT), Beijing 100029, P. R. China*

**Jiahao Liu** − *Beijing Bioprocess Key Laboratory and State Key Laboratory of Chemical Resource Engineering, College of Life Science and Technology, Beijing University of Chemical Technology (BUCT), Beijing 100029, P. R. China*

**An'nan Chen** − *Beijing Bioprocess Key Laboratory and State Key Laboratory of Chemical Resource Engineering, College of Life Science and Technology, Beijing University of Chemical Technology (BUCT), Beijing 100029, P. R. China*

**Juntao Xu** − *Beijing Bioprocess Key Laboratory and State Key Laboratory of Chemical Resource Engineering, College of Life Science and Technology, Beijing University of Chemical Technology (BUCT), Beijing 100029, P. R. China*

**Renwei Zhang** − *Beijing Bioprocess Key Laboratory and State Key Laboratory of Chemical Resource Engineering, College of Life Science and Technology, Beijing University of Chemical Technology (BUCT), Beijing 100029, P. R. China*

**Fang Wang** − *Beijing Bioprocess Key Laboratory and State Key Laboratory of Chemical Resource Engineering, College of Life Science and Technology, Beijing University of Chemical Technology (BUCT), Beijing 100029, P. R. China*

Complete contact information is available at: https://pubs.acs.org/10.1021/acs.joc.0c02995


### Notes

The authors declare no competing financial interest.

## ■ ACKNOWLEDGMENTS

This study was funded by the National Key Research and Development Program of China (2017YFB0306904) and the National Natural Science Foundation of China (Grant nos. 21978017, 21978019, and 21978020).

## ■ REFERENCES


(1) Di, X.; Zhang, Y.; Fu, J.; Yu, Q.; Wang, Z.; Yuan, Z. Ionic Liquid-Strengthened Immobilized *Rhizomucor miehei* Lipase for Catalytic Esterification of Itaconic Acid in Aqueous Media. *ACS Sustainable Chem. Eng.* **2020**, *8*, 1805−1812.

(2) Cordes, T.; Michelucci, A.; Hiller, K. Itaconic acid: the surprising role of an industrial compound as a mammalian antimicrobial metabolite. *Annu. Rev. Nutr.* **2015**, *35*, 451−473.

(3) (a) Daniels, B. P.; Kofman, S. B.; Smith, J. R.; Norris, G. T.; Snyder, A. G.; Kolb, J. P.; Gao, X.; Locasale, J. W.; Martinez, J.; Gale, M., Jr The nucleotide sensor ZBP1 and kinase RIPK3 induce the enzyme IRG1 to promote an antiviral metabolic state in neurons. *Immunity* **2019**, *50*, 64−76. e4 (b) Nair, S.; Huynh, J. P.; Lampropoulou, V.; Loginicheva, E.; Esaulova, E.; Gounder, A. P.; Boon, A. C.; Schwarzkopf, E. A.; Bradstreet, T. R.; Edelson, B. T.; et al. Irg1 expression in myeloid cells prevents immunopathology during *M. tuberculosis* infection. *J. Exp. Med.* **2018**, *215*, 1035−1045.

(4) Mills, E. L.; Ryan, D. G.; Prag, H. A.; Dikovskaya, D.; Menon, D.; Zaslona, Z.; Jedrychowski, M. P.; Costa, A. S.; Higgins, M.; Hams,

E.; et al. Itaconate is an anti-inflammatory metabolite that activates Nrf2 via alkylation of KEAP1. *Nature* **2018**, *556*, 113.
(5) Hooftman, A.; O'Neill, L. A. The immunomodulatory potential of the metabolite itaconate. *Trends immunol.* **2019**, *40*, 687−698.
(6) Bambouskova, M.; Gorvel, L.; Lampropoulou, V.; Sergushichev, A.; Loginicheva, E.; Johnson, K.; Korenfeld, D.; Mathyer, M. E.; Kim, H.; Huang, L.-H.; et al. Electrophilic properties of itaconate and derivatives regulate the IκBζ−ATF3 inflammatory axis. *Nature* **2018**, *556*, 501−504.
(7) Robledinos-Antón, N.; Fernández-Ginés, R.; Manda, G.; Cuadrado, A. Activators and inhibitors of NRF2: a review of their potential for clinical development. *Oxid. Med. Cell. Longevity* **2019**, *2019*, No. 9372182.
(8) O'Neill, L. A.; Artyomov, M. N. Itaconate: the poster child of metabolic reprogramming in macrophage function. *Nat. Rev. Immunol.* **2019**, *19*, 273−281.
(9) Teng, X.; Brown, J.; Choi, S. C.; Li, W.; Morel, L. Metabolic determinants of lupus pathogenesis. *Immunol. Rev.* **2020**, *295*, 167−186.
(10) Olagnier, D. P.; Farahani, E.; Thyrsted, J.; Cadanet, J. B.; Herengt, A.; Idorn, M.; Hait, A.; Hernaez, B.; Knudsen, A.; Iversen, M. B.; et al. Identification of SARS-CoV2-mediated suppression of NRF2 signaling reveals a potent antiviral and anti-inflammatory activity of 4-octyl-itaconate and dimethyl fumarate. *Nat. Commun.* **2020**, *11*, No. 4938.
(11) Sun, X.; Wang, T.; Cai, D.; Hu, Z.; Liao, H.; Zhi, L.; Wei, H.; Zhang, Z.; Qiu, Y.; Wang, J.; et al. Cytokine storm intervention in the early stages of COVID-19 pneumonia. *Cytokine Growth Factor Rev.* **2020**, *53*, 38−42.
(12) Pérocheau Arnaud, S.; Andreou, E.; Pereira Köster, L. V.; Robert, T. Selective Synthesis of Monoesters of Itaconic Acid with Broad Substrate Scope: Biobased Alternatives to Acrylic Acid? *ACS Sustainable Chem. Eng.* **2020**, *8*, 1583−1590.
(13) Leiva, A.; Gargallo, L.; González, A.; Radic, D. Poly (itaconates) monolayers behavior at the air/water interface. Study at different surface concentration. *Eur. Polym. J.* **2004**, *40*, 2349−2355.
(14) Richard, J.-V.; Delaite, C.; Riess, G.; Schuller, A.-S. A comparative study of the thermal properties of homologous series of crystallisable n-alkyl maleate and itaconate monoesters. *Thermochim. Acta* **2016**, *623*, 136−143.
(15) Jala, R. C. R.; Hu, P.; Yang, T.; Jiang, Y.; Zheng, Y.; Xu, X. Lipases as biocatalysts for the synthesis of structured lipids. *Methods Mol. Biol.* **2012**, *861*, 403−433.
(16) Jensen, R. G.; Galluzzo, D. R.; Bush, V. J. Selectivity is an important characteristic of lipases (acylglycerol hydrolases). *Biocatalysis* **1990**, *3*, 307−316.
(17) Zhang, X.; Wan, X.; Cao, H.; Dewil, R.; Deng, L.; Wang, F.; Tan, T.; Nie, K. Chemo-enzymatic epoxidation of *Sapindus mukurossi* fatty acids catalyzed with Candida sp. 99−125 lipase in a solvent-free system. *Ind. Crops Prod.* **2017**, *98*, 10−18.
(18) Wang, M.; Dewil, R.; Maniatis, K.; Wheeldon, J.; Tan, T.; Baeyens, J.; Fang, Y. Biomass-derived aviation fuels: Challenges and perspective. *Prog. Energy Combust. Sci.* **2019**, *74*, 31−49.
(19) Chahinian, H.; Snabe, T.; Attias, C.; Fojan, P.; Petersen, S. B.; Carrière, F. How gastric lipase, an interfacial enzyme with a Ser-His-Asp catalytic triad, acts optimally at acidic pH. *Biochemistry* **2006**, *45*, 993−1001.
(20) Sun, M.; Nie, K.; Wang, F.; Deng, L. Optimization of the Lipase-Catalyzed Selective Amidation of Phenylglycinol. *Front. Bioeng. Biotechnol.* **2020**, *7*, No. 486.
(21) Hamberg, A.; Maurer, S.; Hult, K. Rational engineering of Candida antarctica lipase B for selective monoacylation of diols. *Chem. Commun.* **2012**, *48*, 10013−10015.
(22) Klibanov, A. M. Improving enzymes by using them in organic solvents. *Nature* **2001**, *409*, 241−246.
(23) Duan, Z.-Q.; Du, W.; Liu, D.-H. The mechanism of solvent effect on the positional selectivity of *Candida antarctica* lipase B during 1, 3-diolein synthesis by esterification. *Bioresour. Technol.* **2011**, *102*, 11048−11050.
(24) Bellot, J. C.; Choisnard, L.; Castillo, E.; Marty, A. Combining solvent engineering and thermodynamic modeling to enhance selectivity during monoglyceride synthesis by lipase-catalyzed esterification. *Enzyme Microb. Technol.* **2001**, *28*, 362−369.
(25) Pyo, Y. G.; Hong, S. I.; Kim, Y.; Kim, B. H.; Kim, I. H. Synthesis of monoacylglycerol containing pinolenic acid via stepwise esterification using a cold active lipase. *Biotechnol. Prog.* **2012**, *28*, 1218−1224.
(26) Stergiou, P.-Y.; Foukis, A.; Filippou, M.; Koukouritaki, M.; Parapouli, M.; Theodorou, L. G.; Hatziloukas, E.; Afendra, A.; Pandey, A.; Papamichael, E. M. Advances in lipase-catalyzed esterification reactions. *Biotechnol. Adv.* **2013**, *31*, 1846−1859.
(27) Pereira, C. C.; da Silva, M. A.; Langone, M. A. Enzymatic synthesis of monolaurin. *Appl. Biochem. Biotechnol.* **2004**, *114*, 433−445.
(28) Kang, J. W. Molecular Modeling and its Experimental Verification for the Catalytic Mechanism of *Candida antarctica* Lipase B. *J. Microbiol. Biotechnol.* **2007**, *17*, 1098−1105.
(29) Cao, H.; Wang, M.; Deng, L.; Liu, L.; Schwaneberg, U.; Tan, T.; Wang, F.; Nie, K. Sugar-improved enzymatic synthesis of biodiesel with *Yarrowia lipolytica* lipase 2. *Energy Fuels* **2017**, *31*, 6248−6256.
(30) Lefebvre, C.; Rubez, G.; Khartabil, H.; Boisson, J.-C.; Contreras-García, J.; Hénon, E. Accurately extracting the signature of intermolecular interactions present in the NCI plot of the reduced density gradient versus electron density. *Phys. Chem. Chem. Phys.* **2017**, *19*, 17928−17936.
(31) Finnveden, M.; Semlitsch, S.; He, O.; Martinelle, M. Mono-substitution of symmetric diesters: selectivity of *Mycobacterium smegmatis* acyltransferase variants. *Catal. Sci. Technol.* **2019**, *9*, 4920−4927.
(32) Sharma, S.; Kanwar, S. S. Organic solvent tolerant lipases and applications. *Sci. World J.* **2014**, *2014*, No. 625258.
(33) Kumar, A.; Dhar, K.; Kanwar, S. S.; Arora, P. K. Lipase catalysis in organic solvents: advantages and applications. *Biol. Proced. Online* **2016**, *18*, No. 2.
(34) Dettori, L.; Jelsch, C.; Guiavarc'h, Y.; Delaunay, S.; Framboisier, X.; Chevalot, I.; Humeau, C. Molecular rules for selectivity in lipase-catalysed acylation of lysine. *Process Biochem.* **2018**, *74*, 50−60.
(35) Ferrari, F.; Paris, C.; Maigret, B.; Bidouil, C.; Delaunay, S.; Humeau, C.; Chevalot, I. Molecular rules for chemo-and regio-selectivity of *Candida antarctica* lipase B in peptide acylation reactions. *J. Mol. Catal. B: Enzym.* **2014**, *101*, 122−132.
(36) Li, J.; Zhao, J.; Wang, X.; Qayum, A.; Hussain, M. A.; Liang, G.; Hou, J.; Jiang, Z.; Li, A. Novel angiotensin converting enzyme inhibitory peptides from fermented bovine milk started by *Lactobacillus helveticus* KLDS. 31 and *Lactobacillus casei* KLDS. 105: Purification, identification and interaction mechanism. *Front. Microbiol.* **2019**, *10*, No. 2643.
(37) Liu, C.; Tian, J.; Zhang, R.; Xu, J.; Nie, K.; Deng, L.; Wang, F. Solvent-Free Alcoholysis of Tripalmitin to Produce 2-Monoglyceride as Precursor for 1, 3-Oleoyl-2-Palmitoylglycerol. *Appl. Biochem. Biotechnol.* **2020**, *190*, 867−879.


https://doi.org/10.1021/acs.joc.0c02995
J. Org. Chem. 2021, 86, 7895−7903